

Depth dependent decoherence caused by surface and external spins for NV centers in diamond

Wenlong Zhang, Jian Zhang, Junfeng Wang, Fupan Feng, Shengran Lin, Liren Lou, Wei Zhu* and Guanzhong Wang*

*Key Laboratory of Strongly-Coupled Matter Physics,
Chinese Academy of Sciences,
and Hefei National Laboratory for Physical Science at Microscale,
and Department of Physics,
University of Science and Technology of China. Hefei,
Anhui, 230026, P.R.China.*

By efficient nanoscale plasma etching, the nitrogen-vacancy (NV) centers in diamond were brought to the sample surface step by step successfully. At each depth, we used the relative ratios of spin coherence times before and after applying external spins on the surface to present the decoherence, and investigated the relationships between depth and ratios. The values of relative ratios declined and then rised with the decreasing depth, which was attributed to the decoherence influenced by external spins, surface spins, discrete surface spin effects and electric field noise. Moreover, our work revealed a characteristic depth at which the NV center would experience relatively the strongest decoherence caused by external spins in consideration of inevitable surface spins. And the characteristic depth was found depending on the adjacent environments of NV centers and the density of surface spins.

I. Introduction

The negatively charged nitrogen-vacancy (NV) center in diamond has attracted broad interest owing to its prominent properties. One particular property is the long room-temperature spin coherence time, which is essential for NV centers being used in various applications. Recently, the use of NV centers as sensors to detect external spins [1–6] has been demonstrated, and both the coherence time and detected signal strength are found to be critically dependent on the depth of the NV center [1, 2, 7–11]. In view of this, the depth dependent properties of NV centers as well as the preparation methods of NV centers of different depths have been widely investigated.

Conventionally, low-energy nitrogen-implantation[12] and the epitaxial growth of a high quality nitrogen-doped CVD diamonds followed by electron [13] or ion irradiation [14] are the methods to make shallow NV centers. Moreover, in order to bring an NV center closer to the diamond surface step by step to investigate the depth dependence of its properties, thermal oxidation[11, 15, 16] and plasma etching [16–19] methods have been developed and widely used in the recent years. Compared with thermal oxidation which performs an etching on the entire diamond sample surface, plasma etching method makes it possible to etch a specific area of the sample by previously depositing a mask on the surface [19].

In this paper, we performed plasma etching on a bulk diamond to precisely control the depth of NV centers with respect to the sample surface. Then we studied depth dependence of spin coherence times of the NV centers for samples with external nuclear or electronic spin baths around the surface. In particular, by using NV cen-

ter array and position marks, we could track the very same single NV center at different depths, which enabled us to keep a stable internal adjacent environment of the center and made the depth and external spins the only two variables.

II. Methods

We used an electronic grade (100)-oriented, $2 \times 2 \times 0.5 \text{ mm}^3$ sized diamond substrate from Element Six ($[^{13}\text{C}]=1.1\%$, $[\text{N}]<5\text{ppb}$) for the experiments. By using electron beam lithography, an array made of 60 nm diameter apertures, enclosed with $2 \mu\text{m}$ wide vacant strips (serving also as position marks [11, 20]), were patterned on a 300 nm thick polymethyl methacrylate (PMMA) layer previously deposited on the diamond plate surface [21]. The NV center array in the diamond was created by ion implantation with the $^{14}\text{N}_2^+$ molecule energy of 50 keV and a fluence of $0.65 \times 10^{11} \text{ }^{14}\text{N}_2^+$ per cm^2 through the apertures and strips on the PMMA layer. The implanted sample was annealed at 1050°C in vacuum at $2 \times 10^{-5} \text{ Pa}$ for 2 h to form long spin coherence time centers [22]. Then the sample, after oxidation for 2 h in air at 430°C , was cleaned with acidic mixture (sulfuric, nitric, and perchloric acid in a 1 : 1 : 1 ratio) at 200°C for 1.5 hours.

The plasma-related processes were performed using an ICP RIE reactor (Oxford PlasmaPro NGP80 machine equipped with ICP source). In order to obtain an efficient etching rate, we performed the plasma etching on the diamond sample in conditions of 200 W ICP power, 30 mTorr chamber pressure, 10 sccm of oxygen, 5 sccm of argon, which was different from that used in the previous works [16, 18, 19]. By depositing a mask (lithography-patterned AZ 6112 photoresist) on a part of the sample's surface to protect it from etching, we could get a reference point of the initial depth, with respect to which we could determine the etching rate and depth from surface

* Corresponding authors: gzwang@ustc.edu.cn; zhuw@ustc.edu.cn

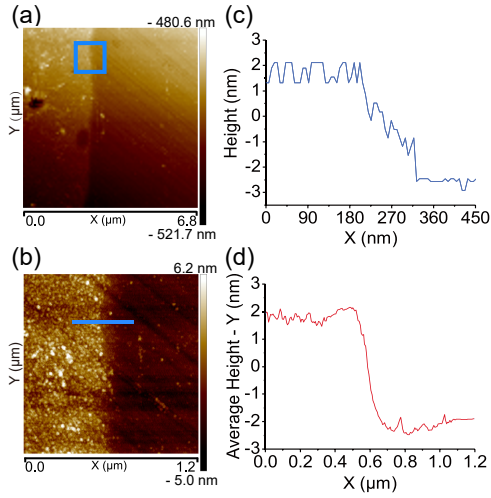


Figure 1. Surface morphology of the etched diamond sample characterized by AFM. (a) Image of a representative area of the substrate etched for 20 seconds. (b) Magnified image of the square area delineated in (a). (c) The distribution of height along the blue line in (b). (d) The distribution along X axis of the Y-axis-average height of the whole area in (b).

topography analysis with the atomic force microscope (AFM). Fig.1 demonstrates a representative result for sample of 20 s etching time. Fig.1(a) shows a $6.8 \times 6.8 \mu\text{m}^2$ area of the etched diamond sample surface, which demonstrates a clear boundary near the middle left. A plane fit was performed on the $1.2 \times 1.2 \mu\text{m}^2$ square delineated in Fig.1(a) to eliminate the effect of slant angle caused by placing sample non horizontally. The resulting corrected image is presented in Fig.1(b). The distribution of height along the randomly selected blue line in Fig.1(b) is shown in Fig.1(c), which indicates an etching depth of about 4 nm at the boundary. After removing remarkable spikes and streaks, the distribution along X axis of the Y-axis-average height is shown in Fig.1(d) from which an etching depth of about 3.8 nm can be obtained. Deriving the etching depths for ten etching experiments of different etching times, we found that the etching rate under the conditions mentioned above was $11.8 \pm 1 \text{ nm/min}$. Therefore, we determined to perform a 20-second plasma etching on the sample (corresponding to an etching depth of about 4 nm) each time when the NV centers were distant from the surface, and a short etching time (corresponding to the etching depths of about 2 nm or 1 nm) when they were shallow. In this way, we made the centers approaching to the sample surface step by step until the centers disappeared, from which the initial depths of NV centers could be derived.

We tracked 227 single NV centers to investigate the distribution of center depth. Respectively, Fig.2(a), (b) and (c) show the fluorescence images of the same representative region of the tracked area of the sample etched for three different etching times (corresponding to the etching depths 0 nm, 20 nm, 44 nm). The strip-shaped bright regions on the left and up sides of the images, im-

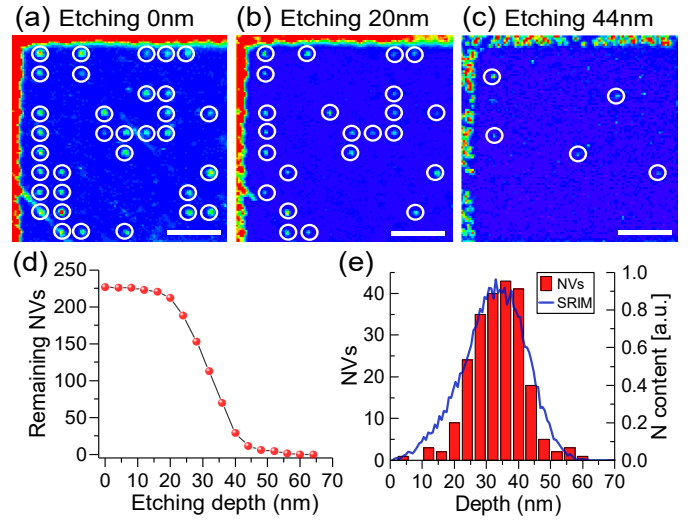


Figure 2. (a), (b) and (c) fluorescence images of the remaining NVs at different etching depths (all with the $5 \mu\text{m}$ scale bar). (a) Image of a representative area of the sample before plasma etching. (b) and (c) The same area after plasma etching for 20 nm and 44 nm, respectively. The tracked single centers are circled. (d) The number of remaining NV centers in the tracked area at different etching depths. (e) The distribution histogram of the number of NVs of different depths, and the SRIM simulated depth profiles (blue curve) of the 25 keV implanted nitrogen atoms.

plying where NV center clusters exist, correspond to the position marks, and the lightspots in white circles represent the tracked single NV centers. Obviously, after etching 20 nm, the position mark strips became less bright, and only 23 centers among the initially tracked 33 single NV centers remained discernible. And after etching 44 nm, the bright strips became interrupted and much less bright, and only 5 single NV centers remained. The evolution of the remaining number of all 227 tracked single NV centers are shown in Fig.2(d). We found that the number of remaining centers reduced slightly when etching depth was 20 nm or less. However, when the etching depth increased further, in a range from 20 to 40 nm, the number reduced dramatically. Finally, when the etching depth was above 40 nm, the number reduced slowly again. By subtracting the numbers of adjacent etching depths, the distribution histogram was obtained and shown in Fig.2(e) which corresponded to the SRIM simulation for an implantation nitrogen atom energy of 25 keV. The result supported our estimated etching rate mentioned above.

III. Results

At each depth, spin coherence times were measured both before and after applying external spins to the diamond surface. The two liquids used were microscope immersion oil and Cu^{2+} solution, providing external nuclear[23] and electronic[6] spins respectively (Though Cu^{2+} provides nuclear spins as well, the electronic spin leads the main effect for decoherence due to

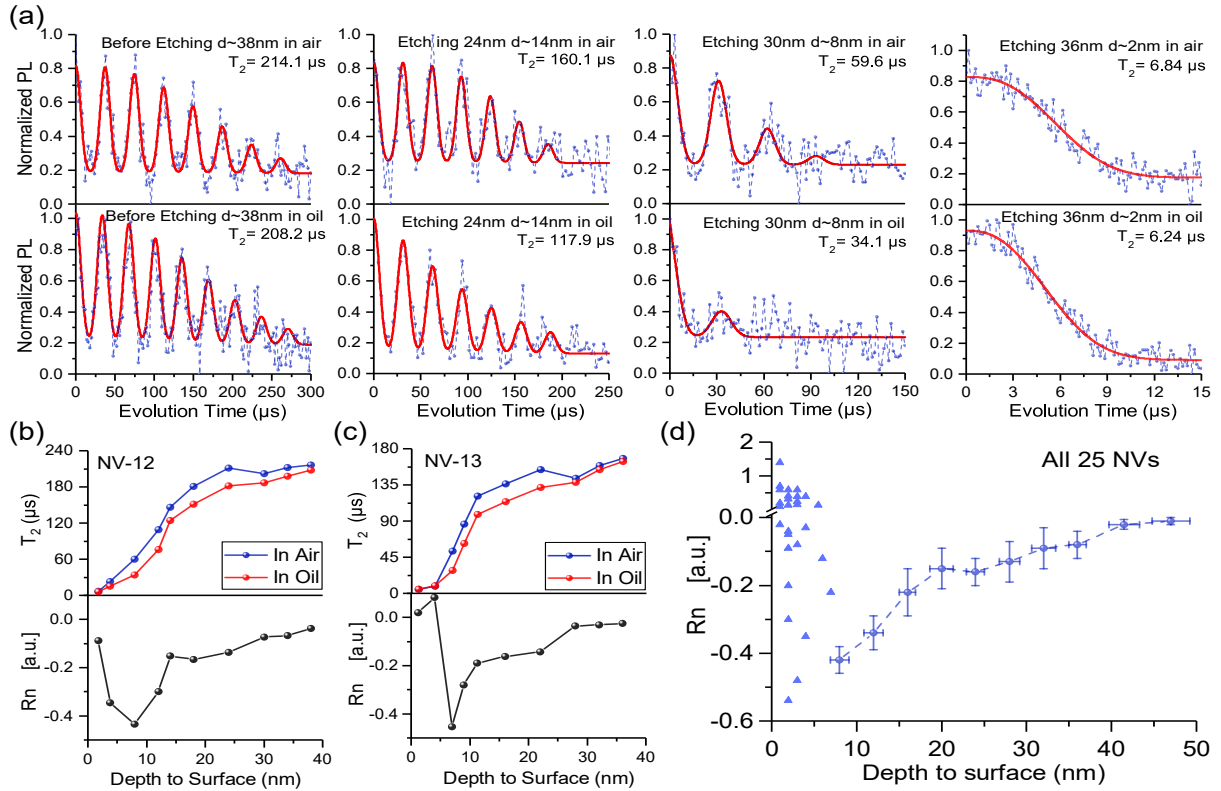


Figure 3. Coherence time measurements of NV centers at different etching depth before and after applying oil. (a) Spin echo measurements of NV-12 at four different etching depths, with surface in air atop, in oil at bottom. (b) and (c) The coherence times of NV-12 and NV-13, respectively, for various depths to the sample surface before and after oil applied, atop; and the R_n at bottom. (d) The R_n of all 25 measured NV centers vs. depths to the sample surface (A few data points under 6 nm are overlapped).

the higher gyromagnetic ratio). The sample was placed in custom built confocal microscope system with the applied magnetic field ($B = 55 \pm 5$ G) paralleling to the detected single NV center axes. Twenty five single centers (labeled NV-01 ~ 25) were randomly selected for the measurements, and initially, the T_2 of three centers of them were less than $50 \mu s$ while of the rest were between 120 to $250 \mu s$, indicating that most of the selected centers were deep inside the sample with a spin bath environment of ^{13}C impurities [24].

Fig.3 exhibits the results of coherence times of the sample with microscope immersion oil applied on the surface. It has been acknowledged that when the surface is exposed to air, the coherence time will decline as NVs approaching to the surface, owing to the influence of surface spin baths existing naturally [10, 25–27] (Since it was difficult to remove the surface spins completely). The coherence times obtained with no external liquid applied to the surface would be called T_2^{air} (which served as a reference), and that with oil applied would be called T_2^{oil} . Noteworthy, we used the ratio $R_n = (T_2^{oil} - T_2^{air}) / T_2^{air}$ to represent the decoherence caused by external nuclear spins, which reflected the intensity of interaction between NV and external nuclear spins with respect to the inevitable intrinsic spins around the diamond surface. Fig.3(a) shows four representative results of spin

echo measurements of NV-12 at different depths. This center disappeared after etching 38 nm, indicating its initial depth to be $d \sim 38$ nm. Before etching, the T_2^{air} of NV-12 was $214.1 \mu s$. After applying oil to the surface, the coherence time T_2^{oil} changed to $208.2 \mu s$, and R_n was about -0.03, suggesting that the external nuclear spins had little influence on the coherence time of the center located at a depth about 38 nm. Then, after etching 24 nm ($d \sim 14$ nm), the T_2^{air} declined to $160.1 \mu s$, and T_2^{oil} declined to $117.9 \mu s$, making R_n to be -0.26, indicating the external nuclear spins indeed had huge effect on coherence time when NVs became shallow. Even more, T_2^{air} and T_2^{oil} of the same center declined to 59.6 and $34.1 \mu s$, respectively, for sample etched for 30 nm, which corresponded to a depth of NV-12 $d \sim 8$ nm. The R_n reduced to -0.43 which meant the external nuclear spins caused strong decoherence. Then, another 30-second-etching was performed to make NV-12 only about 2 nm to the surface, which caused T_2^{air} declined to $6.84 \mu s$, T_2^{oil} to $6.24 \mu s$. However, we found that for the sample thus treated, the R_n increased to -0.09. The T_2^{air} and T_2^{oil} of NV-12 for various depths to the sample surface are presented in Fig.3(b) top, and they both have similar evolution with decreasing depth. As shown in the figure, both T_2^{air} and T_2^{oil} decreased slowly at the depth above 20 nm, then decreased rapidly until NV-12 finally disap-

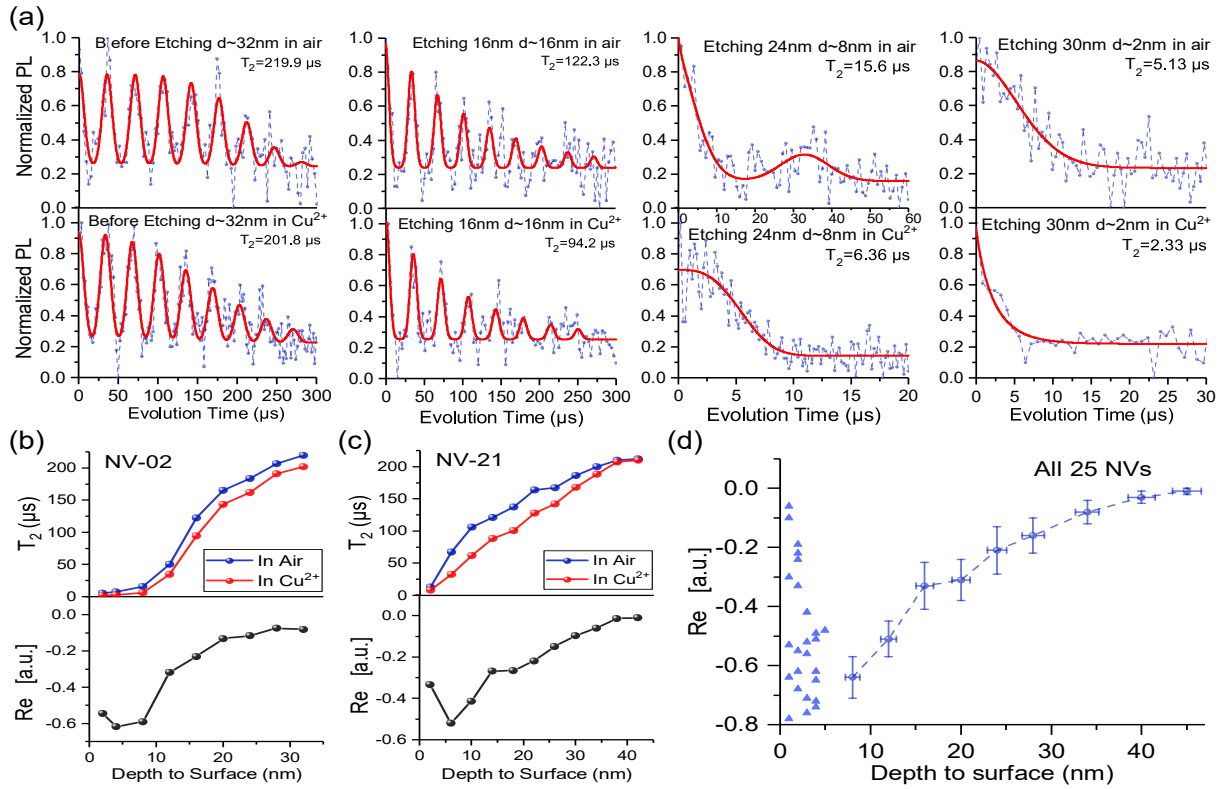


Figure 4. Coherence time measurements of NV centers at different etching depth before and after applying Cu^{2+} solution. (a) Spin echo measurements of NV-02 at four different etching depths, with surface in air atop, in Cu^{2+} solution at bottom. (b) and (c) The coherence times of NV-02 and NV-21, respectively, for various depths to the sample surface before and after Cu^{2+} solution applied, atop; and Re at bottom. (d) All 25 measured NV centers' Re vs. depths to the sample surface.

peared, which was the same as our previous work [11]. Besides, the T_2^{oil} is less than T_2^{air} , revealing the external nuclear spins have enormous influence on coherence time in most cases in addition to intrinsic surface spins. The Rn for the center with various depths are presented in Fig.3(b) bottom, which shows that the Rn curve goes down with the center depth reducing till about 8 nm and then rises. Another representative result of coherence time measurements of single center NV-13 is shown in Fig.3(c). Similar to NV-12, both T_2^{air} and T_2^{oil} of NV-13 decreased slowly with the decrease of its depth in the range above 15 nm, and decreased rapidly in the last 20 nm etching. However, the values of Rn at the depths very near the surface were positive, 0.03 and 0.12 (meaning T_2 increased when external nuclear spins applied), suggesting the decoherence was suppressed by applying oil on the surface.

We summarized the depth dependent Rn of all 25 NV centers in Fig.3(d). For depth above 6 nm, we divided the depth range into sequential intervals (4 nm for the first 8 intervals, and 6 nm for the last 3 intervals), and figured out the mean Rn in every interval. The obtained mean Rn declined from -0.01 to -0.42 with the depth decreasing. For depth under 6 nm, the data of all 25 NVs scattered between -0.54 and 1.43, most around 0.2, revealing that the decoherence caused by applied oil was

unsteady, even suppressed when NVs were very near the surface. The result will be discussed in detail in the following part.

Fig.4 exhibits the results of coherence times with Cu^{2+} solution (providing external electronic spins) applied on the sample surface. Likewise, the ratio $Re = (T_2^{Cu^{2+}} - T_2^{air}) / T_2^{air}$ was used to represent the variation of coherence times caused by external electronic spins. Spin echo measurements of NV-02 with four representative etching depths are shown in Fig.4(a). The center NV-02 initially sat at $d \sim 32$ nm, according to the fact that it disappeared after etching 32 nm. Before etching, the T_2^{air} of NV-02 was $219.9 \mu s$. After applying Cu^{2+} to the sample surface, T_2 ($T_2^{Cu^{2+}}$) changed to $201.8 \mu s$, and Re was about -0.08. After etching 16 nm ($d \sim 16$ nm), the T_2^{air} declined to $122.3 \mu s$, and $T_2^{Cu^{2+}}$ declined to $94.2 \mu s$, making Re to be -0.23. T_2^{air} and $T_2^{Cu^{2+}}$ declined to 15.6 and $6.36 \mu s$ respectively when NV-02 was etched about 8 nm to the surface. Strong decoherence caused by external electronic spins was detected as indicated by the reduced Re of -0.59. However, with etching depth being 30 nm in total, NV-02 was only about 2 nm to the surface, and T_2^{air} and $T_2^{Cu^{2+}}$ declined to 5.13 and $2.33 \mu s$, respectively, making Re changed to -0.55. The T_2^{air} and $T_2^{Cu^{2+}}$ of NV-02 for various depths to the sample surface

are presented in Fig.4(b) top, and the ratios (Re) of them are in Fig.4(b) bottom. Fig.4(c) shows the results of NV-21. Both figures show that the coherence times declined dramatically when NV centers are under 20 nm, for sample surface with or without Cu^{2+} applied. Furthermore, $T_2^{\text{Cu}^{2+}}$ was less than T_2^{air} at each depth, leading to the fact that Re was negative, indicating decoherence caused by external electronic spins was always existing. We also found that Re of the two NVs increased when they were brought very near the surface by etching the sample surface. Re of all the 25 single NV centers at different depths were demonstrated in Fig.4(d). Similar to the processing of Rn, the data of Re in the figure were also divided into two parts, with depths above and under 6 nm. Compared with the evolution of Rn, Re behaved similarly at the depths above 6 nm, also declined regularly. However, when the depth was less than 6 nm, the data points of Re mostly distributed around -0.6, with a few located in the range from -0.42 to -0.06.

IV. Discussion

The results demonstrated above showed that the interaction between NV centers and external spins varied with NV center depth. We took the evolution of Rn as an instance to elaborate the various reasons leading to the results. For the NV centers in diamond, it is inevitable that surface spin bath exists, which contributes to the decoherence of NV centers along with spins in bulk [10, 25–27]. Correspondingly, the coherence time is as follows :

$$T_2^{\text{air}} = 1 / [\gamma_{\text{NV}}^2 (\overline{B_{\text{bulk}}^2} \tau_{\text{bulk}} + \overline{B_{\text{surf}}^2} \tau_{\text{surf}}) + \frac{1}{2T_1}] \quad (1)$$

If external spins are applied on the surface of diamond, the decoherence would also be influenced by the external spins, in addition to the surface spins and spins in bulk. Thus, T_2 with external spins around the sample surface (T_2^{ext}) can be written in the form :

$$T_2^{\text{ext}} = 1 / [\gamma_{\text{NV}}^2 (\overline{B_{\text{bulk}}^2} \tau_{\text{bulk}} + \overline{B_{\text{surf}}^2} \tau_{\text{surf}} + \overline{B_{\text{ext}}^2} \tau_{\text{ext}}) + \frac{1}{2T_1}] \quad (2)$$

In the above expressions, γ_{NV} is the gyromagnetic ratio of NV center, and $\overline{B_{\text{bulk}}^2}$, $\overline{B_{\text{surf}}^2}$, $\overline{B_{\text{ext}}^2}$ are the MS magnetic field signal produced by internal (bulk), surface and external spins respectively, and τ_{bulk} , τ_{surf} , τ_{ext} are the internal (bulk), surface and external spin baths' autocorrelation times respectively, which can be regarded as constant parameters at a given temperature. Noteworthy, the contribution of $\frac{1}{2T_1}$ to $\frac{1}{T_2}$ is far less than that of various spin noises, so it can be neglected. Then, the expression of ratio can be obtained from Eq.(1) and Eq.(2) as :

$$R = \frac{T_2^{\text{ext}} - T_2^{\text{air}}}{T_2^{\text{air}}} = - \frac{\overline{B_{\text{ext}}^2} \tau_{\text{ext}}}{\overline{B_{\text{bulk}}^2} \tau_{\text{bulk}} + \overline{B_{\text{surf}}^2} \tau_{\text{surf}} + \overline{B_{\text{ext}}^2} \tau_{\text{ext}}} \quad (3)$$

It is worth mentioning again that, by using NV center array and position marks, we could track each particular NV center no matter how the sample surface was etched and the external spins were applied. For each tracked NV center, the internal adjacent environment was unchanged as the center depth is not very shallow. Therefore, the quantity $\overline{B_{\text{bulk}}^2} \tau_{\text{bulk}}$ in Eq.(3) was constant for the tracked NV center, and would be denoted by C_{bulk} hereafter. Moreover, for each kind of spins, the autocorrelation time is invariable, i.e. the τ_{surf} and τ_{ext} in Eq.(3) can be regarded as constants (independent of center depth) as well.

Then we focused on the center depth dependent $\overline{B_{\text{surf}}^2}$ and $\overline{B_{\text{ext}}^2}$. When NVs are distant from the surface, the relationship between $\overline{B_{\text{surf}}^2}$ and center depth can be well described based on a model of a 2D layer of surface $g = 2$ spins in case with the surface exposed to air [10]. In particular, for the (100)-oriented diamond, we have :

$$\overline{B_{\text{surf}}^2} = \sigma \left(\frac{g \mu_0 \mu_B}{4\pi} \right)^2 \left(\frac{3\pi}{8d^4} \right) \quad (4)$$

where d is the NV center depth and σ is the mean surface spin density. We note that besides the variable d and a unknown quantity of σ , the other parameters in Eq.(4) can be combined as a constant, C_{surf} . For the $\overline{B_{\text{ext}}^2}$, using a model of the sample surface covered with liquid of infinite thickness that provides homogeneous external nuclear spins [23], it can be derived:

$$\overline{B_{\text{ext}}^2} = \overline{B_{\text{oil}}^2} = \rho \left(\frac{\mu_0 \hbar \gamma_n}{4\pi} \right)^2 \left(\frac{3\pi}{4d^3} \right) \quad (5)$$

where ρ is the nuclear spin number density, d is the NV center depth, and γ_n is nuclear gyromagnetic ratio. The unknown quantity in Eq.(5) is ρ , the value of which depends on the applied oil. However, the rest parameters besides variable d can also be treated as a constant, C_{ext} . With Eq.(4) and (5) substituted into Eq.(3), a simplified expression of Rn can be obtained :

$$Rn = - \frac{\rho \tau_{\text{ext}} C_{\text{ext}} / d^3}{C_{\text{bulk}} + \sigma \tau_{\text{surf}} C_{\text{surf}} / d^4 + \rho \tau_{\text{ext}} C_{\text{ext}} / d^3} \quad (6)$$

Eq.(6) showed the relationship between Rn and NV center depth. With the estimated values of C_{in} , $\sigma \tau_{\text{surf}}$ and $\rho \tau_{\text{ext}}$ in a reasonable range, Eq.(6) was found to fit the data well. The results of Rn and Re (averaged in each interval) are demonstrated in Fig.5. It is noticed that the data points of Rn at the depth above 10 nm conform to the simulated curve in Fig.5(a), while the data points under 10 nm show a deviation from the simulated curve. Moreover, it can be learnt from Eq.(6) that the positive Rn is nonexistent, which is incompatible with the experiment results when NVs were brought near to the surface. The discrepancy was attributed to the following effects.

Firstly, the surface spin baths can not be simply treated as a 2D uniform layer when NVs are very shallow ($d \leq 10$ nm) owing to the existence of discrete surface spin effect or spin clustering [10], which makes the surface spin density inhomogeneous, and consequently, Eq.(4) is no longer valid. In this case, $\overline{B_{surf}^2}$ becomes sensitive to the surface spin distribution and the denominator value of Eq.(6) fluctuates, leading to the R_n value scattering around the simulated curve. Furthermore, recent works reveal that electric field noise plays a significant role in decoherence of near-surface NV centers [28, 29], so the fact that R_n can have positive values is related to the microscope immersion oil, nonconductor of high dielectric constant ($\kappa = 2.3$), which reduces the electric field noise and suppresses the decoherence [28].

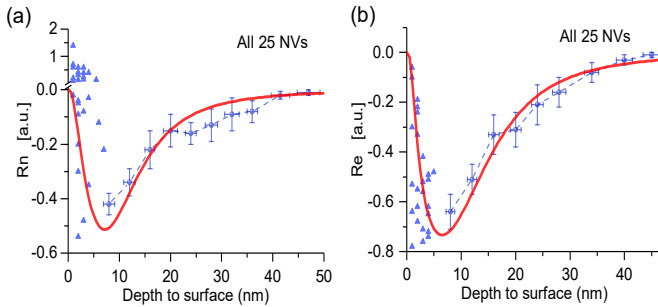


Figure 5. Coherence time ratios of (a) R_n and (b) R_e vs. NV center depths to the sample surface. The solid lines in the figure are simulated curves, which are in red online.

The expression of the ratio R_e ($T_2^{Cu^{2+}} - T_2^{air}$) / T_2^{air} is similar to Eq.(6), and the simulated curve presented in Fig.5(b) demonstrates an appropriate fit with the data. In spite of this, the data deviation from the simulated curve is shown at the depth under 5 nm as well, suggesting that the discrete surface spin effect does influence the values of the ratios. A difference from R_n is that no positive R_e is found, which can be attributed to that the plentiful ions in Cu^{2+} solution near the sample surface would enlarge the electric field [30], instead of decreasing the electric field noise that would suppress the decoherence.

Our results demonstrated that Eq.(6) could explain the depth dependent decoherence behaviours caused by external spins with respect to the inevitable intrinsic spins around the diamond surface. Each simulated curve in Fig.5 shows a minimum at the depth about 6 nm. As an example, by taking the derivative of R_n in Eq.(6) with respect to the center depth d , it was found that R_n would take minimum value at the depth d_0 :

$$d_0 = \sqrt[4]{\frac{\sigma \tau_{surf} C_{surf}}{3C_{bulk}}} \quad (7)$$

Eq.(7) reveals that the characteristic depth (d_0), at

which the ratio R_n (and R_e as well) meets the minimum, only depends on the the adjacent environments of NV centers and the density of diamond surface spins. In external spin detection, the NV center should be brought closing to the sample surface as far as possible to strengthen the detected signal. However, taking surface spins into consideration, the depth at which the external spins cause relatively the most intense decoherence is several nanometers away from the surface. Since the adjacent environment of NV center is changeless, it can be obtained from Eq.(7) that d_0 decreases with σ reducing. Therefore, decreasing the density of surface spins by proper surface treatments can lower d_0 and hence the external spin detection with less influence of surface spins can be realized for the shallow NV center sensors.

V. Summary

We investigated the depth dependence of the coherence times of NV centers for diamond plate with or without external nuclear and electronic spins around the surface. By using NV center array and position marks, each particular NV in the diamond plate etched for different depths could be recognized and tracked. As the internal adjacent environments of the tracked NVs were kept unchanged upon etching, our results obtained by T_2 tracking was more persuasive than that by measuring NVs initially in different depths. We performed plasma etching to control the depths of NVs with an efficient etching rate. Based on this, we applied microscope immersion oil and Cu^{2+} solution on the surface to obtain external nuclear and electronic spins. We introduced the coherence time ratios of R_n and R_e to present the decoherence caused by external spins, and found the depth dependent ratios behaved in the form of a function having a minimum. The characteristic depth at which the NV centers experienced relatively the strongest decoherence caused by external spins, as indicated by the minimum ratio $R = (T_2^{ext} - T_2^{air}) / T_2^{air}$, was found depending on the adjacent environment of NV center and the density of surface spins, which could be useful in the further study and detection of external spins, surface spin noise and so forth with NV centers in diamond.

Acknowledgements

We thank X.X.Wang, J.L.Peng, D.F.Zhou and W.Liu from the USTC Center for Micro- and Nanoscale Research and Fabrication for the technical support of Plasma etching and AFM. We also thank G.P.Guo and J.You from the Key lab of Quantum Information for the support of electron beam lithography. This work was supported by the National Basic Research Program of China (2011CB921400, 2013CB921800) and the National Natural Science Foundation of China (Grant Nos. 11374280, 50772110).

-
- [1] T. Staudacher, F. Shi, S. Pezzagna, J. Meijer, J. Du, C. A. Meriles, F. Reinhard and J. Wrachtrup, *Science*, 2013, **339**, 561–563.
 - [2] H. Mamin, M. Kim, M. Sherwood, C. Rettner, K. Ohno, D. Awschalom and D. Rugar, *Science*, 2013, **339**, 557–560.
 - [3] C. Müller, X. Kong, J.-M. Cai, K. Melentijević, A. Stacey, M. Markham, D. Twitchen, J. Isoya, S. Pezzagna, J. Meijer *et al.*, *Nature communications*, 2014, **5**,.
 - [4] B. Grotz, J. Beck, P. Neumann, B. Naydenov, R. Reuter, F. Reinhard, F. Jelezko, J. Wrachtrup, D. Schweinfurth, B. Sarkar *et al.*, *New Journal of Physics*, 2011, **13**, 055004.
 - [5] F. Shi, Q. Zhang, P. Wang, H. Sun, J. Wang, X. Rong, M. Chen, C. Ju, F. Reinhard, H. Chen *et al.*, *Science*, 2015, **347**, 1135–1138.
 - [6] A. M. Panich, A. Altman, A. I. Shames, V. Y. Osipov, A. E. Aleksenskiy and A. Y. Vul', *Journal of Physics D Applied Physics*, 2011, **44**, 125303.
 - [7] M. S. Grinolds, S. Hong, P. Maletinsky, L. Luan, M. D. Lukin, R. L. Walsworth and A. Yacoby, *Nature Physics*, 2013, **9**, 215–219.
 - [8] D. Rugar, H. J. Mamin, M. H. Sherwood, M. Kim, C. T. Rettner, K. Ohno and D. D. Awschalom, *Nature Nanotechnology*, 2014, **10**, 120–4.
 - [9] T. Häberle, D. Schmidlorch, F. Reinhard and J. Wrachtrup, *Nature Nanotechnology*, 2015, **10**, 125–8.
 - [10] B. A. Myers, A. Das, M. C. Dartiailh, K. Ohno, D. D. Awschalom and A. C. Bleszynski Jayich, *Physical Review Letters*, 2014, **113**, 027602.
 - [11] J. Wang, W. Zhang, J. Zhang, J. You, Y. Li, G. Guo, F. Feng, X. Song, L. Lou and W. Zhu, *Nanoscale*, 2016, **8**, 5780–5785.
 - [12] S. Pezzagna, B. Naydenov, F. Jelezko, J. Wrachtrup and J. Meijer, *New Journal of Physics*, 2010, **12**, –.
 - [13] K. Ohno, F. J. Heremans, L. C. Bassett, B. A. Myers, D. M. Toyli, A. C. B. Jayich, C. J. Palmstrøm and D. D. Awschalom, *Applied Physics Letters*, 2012, **101**, 082413–082413–5.
 - [14] K. Ohno, F. Joseph Heremans, C. F. De, las Casas, B. A. Myers, B. J. Aleman, A. C. Bleszynski Jayich and D. D. Awschalom, *Applied Physics Letters*, 2014, **105**, 383.
 - [15] M. Loretz, S. Pezzagna, J. Meijer and C. Degen, *Applied Physics Letters*, 2014, **104**, 033102.
 - [16] M. Kim, H. J. Mamin, M. H. Sherwood and C. T. Rettner, *Applied Physics Letters*, 2014, **105**, 042406–042406–4.
 - [17] C. Santori, P. E. Barclay, K.-M. C. Fu and R. G. Beausoleil, *Physical Review B*, 2009, **79**, 125313.
 - [18] S. Cui, A. S. Greenspon, K. Ohno, B. A. Myers, A. C. B. Jayich, D. D. Awschalom and E. L. Hu, *Nano letters*, 2015, **15**, 2887–2891.
 - [19] F. Fávoro de Oliveira, S. A. Momenzadeh, Y. Wang, M. Konuma, M. Markham, A. M. Edmonds, A. Denisenko and J. Wrachtrup, *Applied Physics Letters*, 2015, **107**, 073107.
 - [20] J. Wang, F. Feng, J. Zhang, J. Chen, Z. Zheng, L. Guo, W. Zhang, X. Song, G. Guo, L. Fan *et al.*, *Physical Review B*, 2015, **91**, 155404.
 - [21] P. Spinicelli, A. Dréau, L. Rondin, F. Silva, J. Achard, S. Xavier, S. Bansropun, T. Debuisschert, S. Pezzagna, J. Meijer *et al.*, *New Journal of Physics*, 2011, **13**, 025014.
 - [22] T. Yamamoto, T. Umeda, K. Watanabe, S. Onoda, M. Markham, D. Twitchen, B. Naydenov, L. McGuinness, T. Teraji, S. Koizumi *et al.*, *Physical Review B*, 2013, **88**, 075206.
 - [23] L. M. Pham, S. J. DeVience, F. Casola, I. Lovchinsky, A. O. Sushkov, E. Bersin, J. Lee, E. Urbach, P. Cappellaro, H. Park *et al.*, *Physical Review B*, 2016, **93**, 045425.
 - [24] C. Ryan, J. Hodges and D. Cory, *Physical Review Letters*, 2010, **105**, 200402.
 - [25] B. Ofori-Okai, S. Pezzagna, K. Chang, M. Loretz, R. Schirhagl, Y. Tao, B. Moores, K. Groot-Berning, J. Meijer and C. Degen, *Physical Review B*, 2012, **86**, 081406.
 - [26] T. Rosskopf, A. Dussaux, K. Ohashi, M. Loretz, R. Schirhagl, H. Watanabe, S. Shikata, K. Itoh and C. Degen, *Physical review letters*, 2014, **112**, 147602.
 - [27] Y. Romach, C. Müller, T. Uden, L. Rogers, T. Isoda, K. Itoh, M. Markham, A. Stacey, J. Meijer, S. Pezzagna *et al.*, *Physical review letters*, 2015, **114**, 017601.
 - [28] M. Kim, H. Mamin, M. Sherwood, K. Ohno, D. Awschalom and D. Rugar, *Physical review letters*, 2015, **115**, 087602.
 - [29] P. Jamonneau, M. Lesik, J. Tetienne, I. Alvizu, L. Mayer, A. Dréau, S. Kosen, J.-F. Roch, S. Pezzagna, J. Meijer *et al.*, *Physical Review B*, 2016, **93**, 024305.
 - [30] A. N. Newell, D. A. Dowdell and D. H. Santamore, *Journal of Applied Physics*, 2016, **120**, 383–182.